Spin-wave-driven skyrmion dynamics in ferrimagnets: Effect of net angular momentum

Y. Liu,[1] T. T. Liu,[1] Z. Jin,[1] Z. P. Hou,[1] D. Y. Chen,[1] Z. Fan,[1] M. Zeng,[1] X. B. Lu,[1] X. S. Gao,[1] M. H. Qin,[1,*] and J.-M. Liu[1,2]

[1]*Guangdong Provincial Key Laboratory of Quantum Engineering and Quantum Materials and Institute for Advanced Materials, South China Academy of Advanced Optoelectronics, South China Normal University, Guangzhou 510006, China*

[2]*Laboratory of Solid State Microstructures, Nanjing University, Nanjing 210093, China*

(Received 18 April 2022; revised 28 July 2022; accepted 29 July 2022; published 19 August 2022)

Searching for low-power-consuming and highly efficient methods for well-controllable driving of skyrmion motion is one of the most concerning issues for future spintronic applications, raising high concern with the choice of magnetic media and driving scenario. In this work, we propose a scenario of spin-wave-driven skyrmion motion in a ferrimagnetic (FiM) lattice with the net angular momentum δ_s. We investigate theoretically the effect of both δ_s and the circular polarization of the spin wave on the skyrmion dynamics. It is revealed that the momentum onto the skyrmion imposed by the excited spin wave can be partitioned into a ferromagnetic term plus an antiferromagnetic term. The ratio of these two terms and consequently the Hall angle of skyrmion motion can be formulated as the functions of δ_s, demonstrating the key role of δ_s as an effective control parameter for the skyrmion motion. Moreover, the spin wave frequency and chirality dependent skyrmion motion are discussed, predicting the frequency enhanced skyrmion Hall motion. This work thus represents an essential contribution to understanding the skyrmion dynamics in a FiM lattice.

DOI: 10.1103/PhysRevB.106.064424

I. INTRODUCTION

Magnetic skyrmions are particlelike spin textures which are often observed in chiral magnets with Dzyaloshinskii-Moriya interaction (DMI) due to the broken inversion symmetry. Owing to the topologically protected property, skyrmions are rather stable and nanoscale in size [1–5], providing them the possibility to be information carriers in future spintronic devices. Recently, a number of theoretical and experimental studies on skyrmion creation and annihilation [6–10], dynamical manipulation [2,11–13], and fabrication of skyrmion-based devices [14–17] have been reported. For driving the motion of the skyrmion, various technical scenarios are proposed, including those utilizing electric current [12,18,19], magnetic field [20–22], magnetic anisotropy gradient [23,24], etc. While these scenarios show their respective advantages, shortcomings are also a concern. For example, spin-polarized electric current driving always generates Joule heat that is unfavorable. The implementation of the magnetic anisotropy gradient is somewhat limited due to the induced complexity in device integration. The low-power-consuming and highly efficient control scenario for skyrmion motion remains to be one of the most essential issues for potential application of skyrmion spintronics.

For ultralow power consumption, one promising choice is utilization of the spin wave or so-called magnon [25–28] that can drive skyrmion motion without Joule heating and thus is highly preferred [15,29,30]. Moreover, unlike electric current driving, the spin wave as a driving source is free of physical transport of charges and thus is applicable in insulating systems, which is an unbeatable advantage. This motivation has been explored for years and so far the skyrmion motion driven by spin waves in both ferromagnetic (FM) and antiferromagnetic (AFM) media has been investigated. In ferromagnets, by definition the spin wave is only right-circularly polarized because of the broken time-reversal symmetry [31]. This property enables the motion of skyrmions toward the spin wave source in the presence of a transverse motion (i.e., the Hall motion), and the magnon-skyrmion interaction could be viewed as an elastic scattering process where the skyrmion behaves like a massless particle [32,33]. However, for antiferromagnets, spin wave can be either left- or right-circularly polarized [15,31,34], which provides the polarization degrees of freedom including all linear and elliptical polarizations for practical utilization. Indeed, earlier works revealed the dependence of skyrmion motion on the spin-wave polarization in antiferromagnets, and specifically the motion is guided toward the left (right) transverse direction, as driven by the excited right- (left-) handed spin waves. Besides the handedness dependence, it was found that this Hall motion also depends on the linear polarization of the spin wave, as unveiled in our earlier work [35].

While the spin-wave-driven motion of skyrmions in FM and AFM systems has been demonstrated, the as-raised technical issues are also discussed. The strong stray field and relatively slow spin dynamics are disadvantages for a FM system, while effective detection and controllability of an AFM texture are still quite challenging in practice due to the zero net magnetic moment although its high-speed spin dynamics and negligible stray field are highly appreciated. Along this line, a compromise is going to ferrimagnetic (FiM) systems which are under intensive discussion for their preference in future spintronic devices. A FiM lattice has a nonzero net

*qinmh@scnu.edu.cn

moment even around the angular momentum compensation temperature (T_A). While the spin dynamics comparable to antiferromagnets can be reserved if the net angular momentum δ_s is small, the net moment, generally weak in the vicinity of T_A [36–41], can be used as a sensitive parameter to characterize the magnetic state of a FiM system without inducing a large stray field. It is also straightforward to argue that the skyrmion motion and its dynamics in a FiM system would be a generalized extension of the dynamics of skyrmion motions in FM and AFM systems, given $\delta_s = 0$ for an AFM system and sufficiently large δ_s for a FM system.

Therefore, one may choose a proper and nonzero δ_s for probing the magnetic state in a spin-wave-driven skyrmion device made of a FiM system, and thus δ_s appears to be a core control parameter for such device. For example, earlier work demonstrated that the kinetic energy and inertial energy of the Berry phase for a FiM system depends on the δ_s parameter, suggesting a possible modulation of spin dynamics [37–40]. It should be mentioned that the δ_s parameter can be easily adjusted by ion doping or temperature. By this strategy, it is definitely worth exploring how this parameter is used as an additional degree of freedom in controlling the spin-wave-driven skyrmion motion. Given a series of emergent phenomena/effects for such motion in FM and AFM systems [41], our major concern comes to these phenomena in a FiM system in response to the spin wave. This study thus not only uncovers likely additional phenomena but also provides a generalized scenario for skyrmion motion manipulation and device control. For instance, skyrmion Hall motion which is a highly concerned drawback for applications may be suppressed in a FiM system if a suitable δ_s value is chosen.

In fact, skyrmion generation and its motion in FiM materials were observed recently [2,42–45], enhancing the priority for exploring the spin-wave-driven skyrmion motion in a FiM system. In this work, we study the skyrmion motion in a FiM lattice under the stimulation of a circularly polarized spin wave, using theoretical and numerical methods. Net angular momentum δ_s used as the control parameter of the skyrmion motion and the effect of circular polarization (left and right circularly) of the spin wave on the skyrmion motion will be discussed in detail. It is revealed that the motion momentum onto a skyrmion, initiated by an excited spin wave, may be rationally partitioned into two separate terms. One is equivalent to the term existing in a FM lattice and the other is similar to the term existing in an AFM lattice, an expectable outcome. Moreover, it is demonstrated that δ_s as the control parameter determines the ratio of the two terms, which in turn controls the skyrmion Hall motion behavior. The theoretical analysis can be further evidenced by the numerical simulations based on solving the two coupled Landau-Lifshitz-Gilbert (LLG) equations, illustrating the dependence of the Hall angle on δ_s. Finally, the skyrmion dynamics driven by mixed-chirality spin waves is discussed.

II. THEORY FOR SKYRMION DYNAMICS DRIVEN BY CIRCULARLY POLARIZED SPIN WAVES

In this section, we first present a full set of definitions on magnetic structure for a FiM system where two sublattices are usually assumed, and then derive the equations of motion for a skyrmion.

In the continuum framework, the local spin densities are denoted by $\mathbf{s}_1 = s_1\mathbf{n}_1$ and $\mathbf{s}_2 = s_2\mathbf{n}_2$, where $\mathbf{n}_1$ and $\mathbf{n}_2$ are unit vectors of each of the two FiM sublattices; $s_i = M_i/\gamma$ is the magnitude of the spin density; M_i is the magnetization; and $\gamma_i = g_i\mu_B/\hbar$ is the gyromagnetic ratio of sublattice i. For clarity, both s_1 and s_2 are defined to be positive; $s = (s_1 + s_2)/2$ is the spin density average of the two sublattices and thus the net angle momentum $\delta_s = s_1 – s_2$.

Furthermore, one may introduce the staggered vectors $\mathbf{n} = (\mathbf{n}_1 – \mathbf{n}_2)/2$ and $\mathbf{m} = (\mathbf{n}_1 + \mathbf{n}_2)/2$ to deal with the dynamic equations of ferrimagnets. With this set of definitions, one can formulate the dynamic equation of the matter under study.

A. Lagrangian of FiM dynamics

Following earlier work, the FiM dynamic equations can be written in terms of the Néel vector $\mathbf{n}$, whose Lagrangian density is given by [2,36,46,47]

$$L = L_B - U, \tag{1}$$

where L_B is the spin Berry phase and U is the free energy density. The spin Berry phase, which governs the magnetic dynamics, is given by [37]

$$\mathrm{L}_B = \delta_s\mathbf{a}(\mathbf{n})\cdot\dot{\mathbf{n}} + \rho\dot{\mathbf{n}}^2/2, \dot{\mathbf{n}} = d\mathbf{n}/dt, \tag{2}$$

where $\rho = s^2/a$ is the constant of inertia [48] with the homogeneous exchange constant a, $\mathbf{a}(\mathbf{n})$ is the vector potential for the assumed magnetic monopole satisfying $\nabla_{\mathbf{n}} \times \mathbf{a}(\mathbf{n}) = \mathbf{n}$ [12,32]. The first term represents the spin Berry phase associated with δ_s, and the second term represents the dynamic inertia of $\mathbf{n}$. The two terms reflect the ferromagnetic and antiferromagnetic natures of the system, respectively, consistent with the LLG equation.

The free energy density U including the exchange interaction, interfacial Dzyaloshinskii-Moriya interaction (DMI), and uniaxial anisotropy energy, is defined as

$$U = \mathrm{A}(\nabla\mathbf{n})^2 - K\mathbf{n}_z^2 + D[\mathbf{n}_z\nabla\cdot\mathbf{n} - (\mathbf{n}\cdot\nabla)\mathbf{n}_z], \tag{3}$$

where A, K, and D are the approached exchange, anisotropy, and interfacial DMI coefficients, respectively.

In the preceding, one considers the excitation of spin waves in such a FiM system. Usually, this excitation is described by the Néel vector $\mathbf{n}$ that can be divided into two parts [15,26]: (1) the slowly moving texture $\mathbf{n}_0$ and (2) the fast evolving spin-wave excitation component $\mathbf{n}'$; they are called, respectively, the static and dynamic components, and are more conveniently described when local coordinate $\hat{\mathbf{e}}_{\theta,\varphi,r}$ is included [32]. Namely, $\mathbf{n}_0 = \hat{\mathbf{e}}_r$ and $\mathbf{n}' = n_\theta\hat{\mathbf{e}}_\theta + n_\varphi\hat{\mathbf{e}}_\varphi$. A complex expression of this staggered vector reads $\psi(\mathbf{r}, t) = n_\theta + in_\varphi$. Consequently, the spin Berry phase term L_B of the Lagrangian density L and the free energy density U in Eq. (1) are rewritten as

$$\begin{aligned} L_B &= \delta_s\left(a_t^0 - \phi a_t^0\right) + \rho\big[(1-2\phi)\dot{\mathbf{n}}_0^2 \\ &\quad + i(\psi^*\partial_t\psi - \psi\partial_t\psi^*)a_t^0 + \partial_t\psi^*\partial_t\psi\big]/2, \\ U &= u_0 + \mathbf{j}\cdot\mathbf{a}_{\text{total}} - 2\phi u_0 + A\nabla\psi^*\nabla\psi/2 - K\phi, \end{aligned} \tag{4}$$

where $\mathbf{j} = iA(\psi^*\nabla\psi - \psi\nabla\psi^*)/2$ is the flux of spin waves and $\phi = \psi^*\psi/2$ is the local intensity of spin waves; $u_0 = u(\mathbf{n}_0)$ is the local texture energy associated with the moving texture $\mathbf{n}_0$ as the background; $\mathbf{a}_{\text{total}} = \mathbf{a}_0 + \mathbf{a}_D$ is the total vector potential, including the inhomogeneous magnetization and DMI with $a_i^0 = \cos\theta_0\partial_i\phi_0$ being the i component of $\mathbf{a}_0$, and $\mathbf{a}_D = -(D/A)\mathbf{n}_0$ [40]; a_t^0 is the scalar potential associated with the dynamics of spin texture [32,38].

B. Collective coordinate theory

Given the FiM dynamic equations, now one can focus on the skyrmion formation and its motion, as driven by a spin wave. Since the issue to be discussed is on the moving objects, and both skyrmion and spin wave can be treated as rigid texture and quasiparticles moving in the lattice, one needs to construct the collective coordinates for the issue to be discussed.

Generally, a skyrmion can be expressed in the collective coordinates $\mathbf{n}_0(t) = \mathbf{n}_0[\{X_\mu(t)\}]$. For the spin wave, the collective coordinates $\psi(t) = \psi[\{x_i(t)\}]$ are usually employed, as done in wave packet theory [32,46]. Here subscript indices (μ, ν) and (i, j) correspond to the two-dimensional real-space vectors for skyrmion and spin wave packets collective coordinates, respectively. The whole Lagrangian L, here specifically denoted as L_z, can be now represented in terms of $\{X_\mu(t)\}$ and $\{x_i(t)\}$:

$$L_z = \delta_s A_\mu^0(\phi)\dot{X}_\mu + \rho\left[M^{\mu\nu}\dot{X}^2 - 4\omega\rho_{sw}a_\mu^0\dot{X}_\mu + \rho_{sw}\omega^2\right]/2 - U_0(\phi) - \rho_{sw}\left(\Omega_\pm a_i^{\text{total}}\dot{x}_i - \Omega_\pm^2\dot{x}_i\dot{x}_i/4A\right), \quad (5)$$

where $\rho_{\text{sw}} = \int\phi dV$ is the total intensity of the spin waves; $M^{\mu\nu} = (1-2\phi)\int[\partial_\mu\mathbf{n}_0\cdot\partial_\nu\mathbf{n}_0]dV$ is the effective mass of the skyrmion; $A_\mu^0(\phi) = \int(1-\phi)a_t^0 dV \approx A_\mu^0 - \rho_{sw}a_\mu^0(\mathbf{x})$ is the vector potential for coordinate X_μ with $a_\mu^0 = \mathbf{a}(\mathbf{n_0})\cdot\partial_\mu\mathbf{n}_0$; $U_0(\phi) = \int(1-2\phi)u_0 dV \approx U_0 - 2\rho_{sw}u_0(\mathbf{x})$ denoting the total texture energy with $A0\,\mu$ and U_0 being the vector potential and energy of the spin texture (no spin wave component), respectively; and $\dot{\mathbf{x}}$ is the velocity vector of spin wave packet. $\Omega_\pm = \pm(2\rho\omega - \delta_s)$, where $\Omega_+(\Omega_-)$ corresponds to the right-(left-) handed spin wave. It is worth noting that the dynamics of FiM magnons satisfies the Klein-Gordon equation [40], and its energy has a squared-frequency term $\sim\omega^2$.

Given the Lagrangian formulation, one needs to consider the resistance to the motion of objects; i.e., the friction force against the motion which should be proportional linearly to the motion velocity, described as the Rayleigh term R for the dissipation in the collective coordinates:

$$R = s\cdot\alpha[\Gamma_{\mu\nu}\dot{X}_\mu\dot{X}_\nu + 2\rho_{sw}\kappa\dot{x}_i\dot{x}_i]/2,$$
$$\Gamma_{\mu\nu} = (1-2\phi)\int(\partial_\mu\mathbf{n}_0\cdot\partial_\nu\mathbf{n}_0)dV,$$
$$\kappa = \left[(2\rho\omega - \delta_s)^2 - \delta_s^2 - 4\rho K\right]/4A\rho, \quad (6)$$

where $\alpha = (s_1\alpha_1 + s_2\alpha_2)/s$, $s = (s_1 + s_2)/2$.

Subsequently, the motion equations of the skyrmion and spin wave packet in the collective coordinates using the Euler-Lagrangian rule are expressed as

motion equation for skyrmion :

$$\rho M^{\mu\nu}\ddot{X}_\nu = E_\mu^0 + (\delta_s - 2\rho\omega\rho_{sw})B_{\mu\nu}^0\dot{X}_\nu - s\cdot\alpha\Gamma_{\mu\nu}\dot{X}_\nu - \rho_{sw}\Omega_\pm b_{\mu i}\dot{x}_i, \quad (7a)$$

motion equation for spin wave packet :

$$\Omega_\pm^2 m_{sw}\ddot{x}_i = 2e_i - \Omega_\pm b_{ij}\dot{x}_j - 2s\alpha\kappa\dot{x}_i + \Omega_\pm b_{\mu i}\dot{X}_\mu, \quad (7b)$$

where $E_\mu^0 = -\partial_\mu U_0$; $e_i = -\partial_i u_0$; $B_{\mu\nu}^0 = \partial_\mu A_\nu^0(\phi) - \partial_\nu A_\mu^0(\phi)$, $b_{\mu i} = \partial_\mu a_i - \partial_i a_\mu$, and $b_{ij} = \partial_i a_j - \partial_j a_i$ are the effective electromagnetic fields; $m_{sw} = 1/2A^*$ is the normalized effective mass of the wave packet.

Here, it is noted that the two equations are intercorrelated because Eq. (7a) contains a term with the collective coordinates $x_i(t)$ of the spin wave and Eq. (7b) contains a term with the collective coordinates $X_\mu(t)$ of the skyrmion. Particularly, the first and second terms in the right side of Eq. (7a) are associated with the effective electric and magnetic forces acting on the skyrmion respectively, the third term is the drag force, and the last term is the acting force imposed by the excited spin wave. Similarly, the motion of a single spin wave packet is also equivalent to the classical motion of a massive particle, which is determined by the effective forces acting on the wave packet expressed in the right side of Eq. (7b).

Certainly, it would be very useful if one could obtain a set of rigorous solutions to Eq. (7) in terms of the motions of both skyrmion and spin wave packet. However, such a set of solutions seems to be challenging if not impossible, and therefore we may discuss a relatively simplified version of the motion behaviors. One case is to neglect the dissipative components which would be quite weak if the system under investigation can be optimized.

Given this assumption, one can update Eq. (7) for a simplified description of the motions of skyrmion and wave packets in the vector version, by setting the damping factor $\alpha = 0$, yielding

$$\rho M\ddot{\mathbf{X}} = -(2\rho\omega\rho_{sw} - \delta_s)\mathbf{B}^0\times\dot{\mathbf{X}} - \rho_{sw}\Omega_\pm\mathbf{b}\times\dot{\mathbf{x}}, \quad (8a)$$

$$\Omega_\pm m_{sw}\ddot{\mathbf{x}} = -\mathbf{b}\times\dot{\mathbf{x}} + \mathbf{b}\times\dot{\mathbf{X}}, \quad (8b)$$

where $\mathbf{B}^0$ and $\mathbf{b}$ are the equivalent fields acting on the skyrmion and spin wave packet, respectively. $\dot{\mathbf{X}}$ and $\ddot{\mathbf{x}}$ are the velocity and acceleration of the skyrmion, respectively, and $\ddot{\mathbf{x}}$ is the acceleration of thespin wave packet. Equation (8) represents a simplified version of Eq. (7) and the physics associated with the motions of skyrmion and spin wave packet can be seen more clearly from Eq. (8).

Subsequently, we present some qualitative discussion on these motions and the details of theoretical analysis will be presented in Sec. III. As stated above, the motions of skyrmion and spin wave packet are intercorrelated. The spin-wave-driven motion of the skyrmion can be discussed from two aspects. One is to check the scattering of the spin wave packet from the skyrmion, and of course such scattering can be viewed as the counter-resistance of the moving skyrmion against the spin wave as the driving force. The other case is

to check the skyrmion momentum imposed by the spin wave. Discussing the two aspects separately allows us to understand the whole landscape of dynamics of the spin-wave-driven skyrmion motion.

C. Scattering of spin wave packet

Without losing generality, the scattering of the spin wave packet in the present problem can be discussed by assuming the approximately stationary skyrmion, as seen from Eq. (8b), given the much quicker motion of the spin wave packet than the skyrmion. The first term in the right side of Eq. (8b) is the effective Lorentz force acting on the spin wave packet, imposed by the skyrmion, which induces the transverse motion of the packet. This is the dominant term of the spin wave scattering. Moreover, by the definition $\Omega_{\pm} = \pm(2\rho\omega - \delta_s)$, one sees that Ω has the same sign as the wave frequency ω, noting that term $2\rho\omega$ gives the main contribution. In other words, due to $|\delta_s| \ll 2\rho\omega$, the magnitude of $\Omega_{\pm}$ may change linearly with δ_s, but the sign of Ω is determined by the handedness of the spin wave; i.e., positive Ω_+ (negative Ω_-) is obtained for the right- (left-) handed spin wave.

As a result, unless the net angular momentum δ_s is extremely large in magnitude, corresponding to the case of the FM system, the spin wave scattering by the skyrmion in a FiM system would hardly be affected by δ_s. The scattering would likely be similar to the case in an AFM system, as reported in recent works in the literature [15]. However, the skyrmion momentum imposed by the spin wave in a FiM system is rather different from those in FM and AFM systems, as revealed in the following section.

D. Skyrmion momentum

It is well known that for spin-wave-driven skyrmion motion in FM and AFM systems, the skyrmion motion is much slower than the propagation of the spin wave packet. This fact applies to the present FiM system, and thus we first discuss the momentum onto the skyrmion imposed by the spin wave packet. Given the spin Berry phase term L_B defined in Eq. (5), one may start from Eq. (7a) or (8a), to calculate the skyrmion momentum P_μ that is the derivative of L_B with respect to the collective velocity defined by the collective coordinate X_μ [33]:

$$P_\mu = \partial L_B/\partial \dot{X}_\mu = \delta_s A^0_\mu + \rho M^{\mu\nu}\dot{X}_\mu. \tag{9}$$

The two terms constituting momentum P_μ are similar to those derived for the FM lattice and the AFM lattice, which are referred to as the FM term and the AFM term, respectively. Notably, the skyrmion momentum in a FiM system depends on δ_s and this dependence does not exist in the FM or AFM system. Obviously, the first term is linearly related to δ_s and symmetric about the X axis, due to the mirror symmetry [15]. In the second term, parameter ρ monotonously decreases with δ_s; thus this second term is a decreasing function of δ_s.

Consequently, the δ_s parameter can be used as an effective control of the relative weight of the two momentum terms (i.e., their ratio), and eventually it becomes a critical parameter to determine the skyrmion dynamics. For the two limitations $\delta_s \to \infty$ and $\delta_s = 0$, skyrmion dynamics should be similar to those in the FM system and the AFM one, respectively. Importantly, the skyrmion Hall angle can be modulated via tuning δ_s, which is very essential for future applications because the issue of Hall motion has been an issue of high concern and is detrimental for successful applications. Details of these behaviors will be presented below by theoretical analysis and LLG simulations.

III. NUMERICAL ANALYSIS

The theoretical treatment presented above unveils quite a few of the major characteristics of the skyrmion motion as driven by a spin wave of circular polarization (right- or left-handedness). In order to check these predictions, and more importantly in order to apply this theory to a realistic system, one needs to comprehend our understanding of this theory by comparing the theoretical analysis with the numerical simulations based on the standard Heisenberg spin model using the LLG equation. The consistency of the proposed theory with the simulation results would be the criterion for the validity of the dynamic theory.

A. Theoretical analysis

Based on Eq. (8), one notes that the motion of the spin wave packet in connection with the skyrmion is similar to the motion of a classical particle under an effective magnetic field. However, the solutions to Eq. (8) are still challenging to obtain, and we turn to the numerical calculations using the fourth-order Runge-Kutta methods with a time step of 10^{-13} s. The theoretical analysis is performed on a 400 nm $\times$ 400 nm system, in which the spin wave is excited at the left boundary and moves toward the skyrmion locating in the center of the system. As discussed previously, the skyrmion is pinned at this stage, considering the fact that the spin wave travels much faster than the skyrmion.

The velocity of the spin wave can be calculated from the spin wave dispersion. Following the earlier work [29,39,49], we obtain the spin wave dispersion,

$$\omega_{\pm} = \left[\pm\delta_s + \sqrt{\delta_s^2 + 4\rho(Ak^2 + K)}\right]/2\rho, \tag{10}$$

where $\omega_+(\omega_-)$ corresponds to the right- (left-) handed spin wave and k is the wave vector of the spin wave. Then, the speed of the spin wave, $v_{\rm sw}$, is obtained from $v_{\rm sw} = \partial\omega_{\pm}/\partial k$. One notes that the dispersion behavior of spin waves can hardly be affected by DMI as revealed in the earlier works [39], which is attributed to the fact that DMI is negligible for the FiM domain with perpendicular magnetization. Subsequently, the scattering of the spin wave packet is calculated numerically by solving Eq. (8). Without a loss of generality, we set the skyrmion topological number $Q = -1$; the skyrmion size to be 20 nm which corresponds to the case of $A = 15\,\mathrm{pJ/m}$, $D = 1.2\,\mathrm{mJ/m^2}$, and $K = 85\,\mathrm{kJ/m^3}$; and the spin wave frequency to be $\omega = 300\,\mathrm{GHz}$. These parameters are comparable with those as discussed in the literature on compound GdFeCo [7,38].

TABLE I. Parameters used in the numerical simulations.

Index	1	2	3	4	5	6	7	8	9
M_1 (kA/m)	1120	1115	1110	1105	1100	1095	1090	1085	1080
M_2 (kA/m)	1040	1030	1020	1010	1000	990	980	970	960
$\delta_s(\times 10^{-7}\,\mathrm{J\,s/m^3})$	–1.24	–0.93	–0.62	–0.31	0	0.31	0.62	0.93	1.24

B. Model-based simulations

We check and solidify our conclusion by micromagnetic simulations. For the present case, the model Hamiltonian on a generalized spin lattice may be given by

$$H = J\sum_{\mathrm{i}} \mathbf{s}_i \cdot \mathbf{s}_{i+1} + \mathrm{D}^* \sum_i (\mathbf{u}_{ij} \times \hat{z}) \cdot (\mathbf{s}_i \times \mathbf{s}_{i+1}) + K^* \sum_i (\mathbf{s}_i \cdot \hat{z})^2, \tag{11}$$

with the exchange coupling $J = Ad/4$ with the lattice constant d, the interfacial DMI magnitude $D^* = Dd^2/8$, the unit vector $\mathbf{u}_{ij}$ connecting the nearest neighbors, and the anisotropy constant $K^* = Kd^2d_z/2$ with the thickness d_z [44]. The coupling parameters are the same as those in the theoretical analysis. The dynamics of the skyrmion and spin wave packet is investigated by solving the LLG equation,

$$\frac{\partial \mathbf{s}_i}{\partial t} = -\gamma_i \mathbf{s}_i \times \mathbf{H}_{\mathrm{eff},i} + \alpha_i \mathbf{s}_i \times \frac{\partial \mathbf{s}_i}{\partial t}, \tag{12}$$

where $\mathbf{H}_{\mathrm{eff},i} = M_i^{-1}\partial H/\partial \mathbf{s}$ is the effective field with the magnetic moment M_i at site i, the gyromagnetic ratio $\gamma_i = g_i\mu_B/\hbar$ with the g factors [50] $g_1 = 2.2$ and $g_2 = 2$, and the damping constants are set to be $\alpha_1 = \alpha_2 = 0.004$.

For practical simulations based on the LLG equation, we start from a discrete lattice with the size of 400 nm × 400 nm × 7 nm and cell size of 2 nm × 2 nm × 7 nm, and set the time step to 10^{-13} s. The used magnetic moments M_i for nine different cases are shown in Table I [38], and they correspond to nine different δ_s. Here, the spin waves are excited by applying the AC magnetic field in the region of $70\,\mathrm{nm} < x < 80\,\mathrm{nm}$ and $0 < y < 400\,\mathrm{nm}$, which propagate along the x direction. Specifically, we generate right-/left-handed spin waves by applying an AC magnetic field $\boldsymbol{h}_\mathrm{R}/\boldsymbol{h}_\mathrm{L} = h[\cos(\omega_h t)\mathbf{e}_x \pm \sin(\omega_h t)\mathbf{e}_y]$ with amplitude h and the frequency $\omega_h = 300\,\mathrm{GHz}$ [51]. The absorbing boundary conditions are used to eliminate the reflection of the spin waves at the boundary.

C. Comparison between the theoretical and simulated results

Subsequently, we check the consistency of the theoretical analysis based on Eq. (8) with the LLG simulations via the comparison between the numerical and simulated spin wave scattering. One notes that the driving force for skyrmion motion from the spin wave originates from the skyrmion–spin wave interaction, and it is intrinsic from the scattering of the spin wave by the moving skyrmion. This scattering acts reversely on the skyrmion, driving its motion. Therefore, it is necessary to formulate the scattering process and then to discuss the underlying physics.

The Eq. (8) based numerically calculated trajectories of the spin wave packet with right-handedness for various δ_s are shown in Fig. 1(a). It is clearly shown that the right-handed spin wave packet is scattered by the skyrmion toward the negative y direction. With the increase of δ_s, the effective field of the skyrmion increases, which slightly enhances the scattering of the spin wave packet. Oppositely, the left-handed spin wave packet is deflected toward the positive y direction, as clearly shown in Fig. 1(b) where the scattering of the spin wave packet with left-handedness is presented. Thus, the theoretical results demonstrate that the scattering of the spin wave is determined by the wave handedness and hardly affect by δ_s, consistent with the above analysis. This property is also confirmed in our micromagnetic simulations. Figure 2 presents the Bragg intensity from Fourier transformation of the spatiotemporal oscillation of simulated n_x, which describes the spin wave intensity. For the right-handed spin wave, considerable Bragg intensity is observed in the vector region with negative k_y as depicted with red circles in Figs. 2(a)–2(c), confirming that the spin waves are scattered toward the negative y direction by the skyrmion. On the other hand, the left-handed spin waves are deflected toward the positive y direction, resulting in the considerable Bragg intensity in the positive k_y region, as shown in Figs. 2(d)–2(f). Undoubtedly, the simulations are well consistent with the theoretical analysis, confirming the validity of the theoretical analysis above.

While the δ_s parameter only weakly affects the spin wave scattering, its effect on the spin wave intensity is relatively remarkable and depends on the spin wave handedness, as shown in Fig. 2. It is clearly shown that for the right-handed

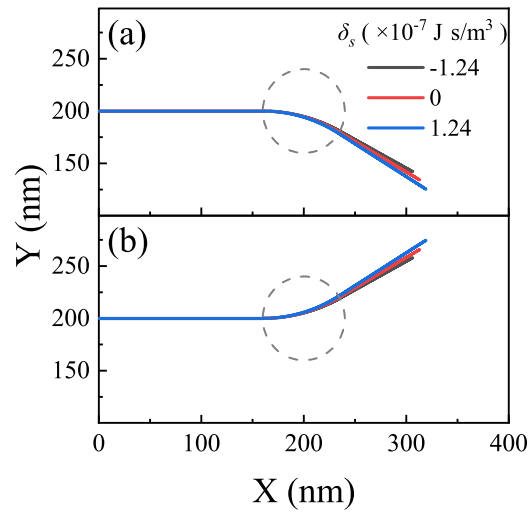

FIG. 1. Skew scattering of (a) right-handed and (b) left-handed spin wave packet across the skyrmion (dashed circle).

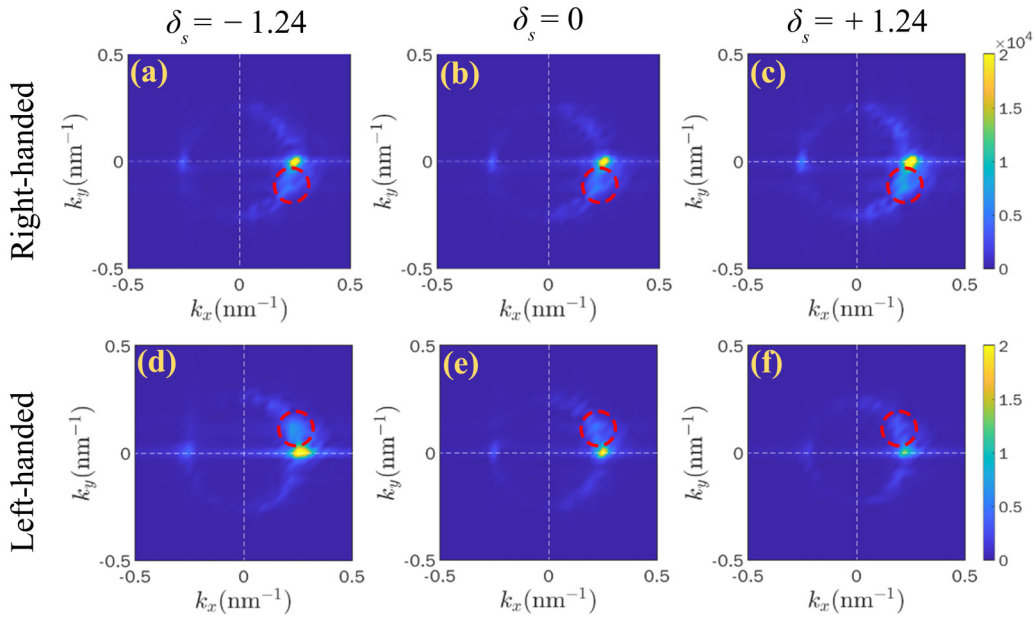

FIG. 2. Spatial fast Fourier transition spectrum for $\omega_h = 300\,\mathrm{GHz}$ for various δ_s in units of $10^{-7}\,\mathrm{J\,s/m^3}$ driven by right-handed spin waves (a–c) and by left-handed spin waves (d–f). Here, the fast Fourier transition analysis is implemented over the whole plane.

spin waves, the wave magnitude increases with increasing δ_s. This effect is attributed to the resonant frequency of the spin wave in FiM systems, which reads

$$\omega_{\pm}^{c} = \left[\sqrt{(a+K)^2\delta_s^2 + (8aK+4K^2)s_1s_2} \pm \delta_s(a+K)\right]/2s_1s_2. \tag{13}$$

Obviously, as the frequency of excitation field ω_h gets close to the resonant frequency, a high-intensity spin wave is excited. Here, ω_+^c is estimated to be ~63 GHz and further increases with increasing δ_s, resulting in the enhancement of spin wave intensity. Reversely, for the left-handed spin wave, ω_-^c decreases and gets far away from ω_h with the increase of δ_s, resulting in the suppression of the spin wave intensity, as shown in Figs. 2(d)–2(f).

As a matter of fact, the scattering of spin waves by skyrmions in FM [33] and AFM [15] systems has been discussed in earlier works. In these systems, the scattering direction or scattering cross section determines the momentum transfer from the spin wave to the skyrmion, which in turn modulates the skyrmion motion, similar to the course of two-particle elastic collision. However, in a FiM system, the case becomes more complex because the relative weight of the two skyrmion momentum terms (i.e., their ratio) significantly depends on δ_s, as revealed in Sec. II D. Thus, it is reasonably expected that δ_s is a critical parameter to determine the skyrmion dynamics including Hall motion, although it hardly affects the scattering of the injected spin wave.

D. Effect of δ_s on skyrmion Hall motion

The consistency of the micromagnetic simulations with the theoretical analysis allows one to clearly uncover the effect of δ_s on the skyrmion dynamics using simulations, noting that a rigorous derivation of the skyrmion velocity is quite challenging.

As predicted in Sec. II D, δ_s can effectively modulate the ratio between the FM momentum term and the AFM term, which in turn tunes the skyrmion Hall motion. This prediction is verified in our micromagnetic simulations, and interesting dynamic behaviors of the skyrmion are revealed. Figure 3(a) presents the trajectory of the skyrmion for various δ_s driven by the right-handed spin waves excited by magnetic field with $h = 600\,\mathrm{mT}$. One notes that the FM momentum term is completely suppressed for $\delta_s = 0$, and the skyrmion dynamics in ferrimagnets are controlled by the AFM term. Thus, strong Hall motion is observed at $\delta_s = 0$, the same as in the AFM system [15], due to the fact that the dynamics of a magnetic texture mainly depends on the net angular momentum. In this case, the FiM skyrmion propagates away from the spin wave source with a strong transverse motion along the $+y$ direction [black squares in Fig. 3(a)].

Furthermore, we quantitatively calculated the Hall angle based on Eq. 8(a) through analyzing the interaction of all wave packets in real space with a skyrmion using the fourth-order Runge-Kutta method. Figure 4(a) gives the theoretical

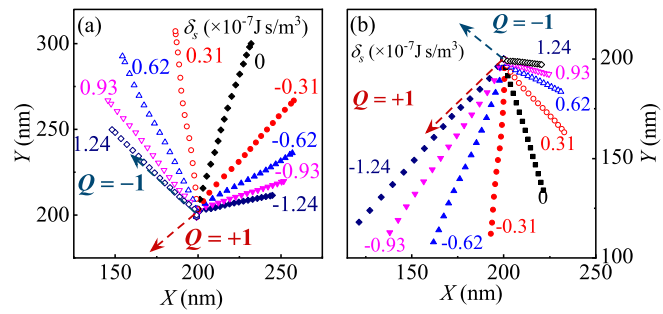

FIG. 3. The trajectory of a skyrmion driven by (a) the right-handed spin waves, and (b) the left-handed spin waves for various δ_s.

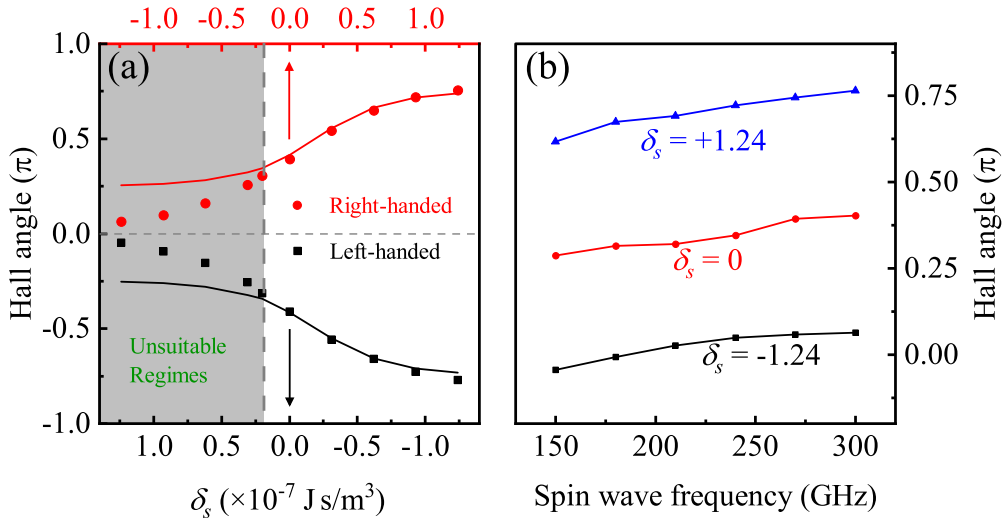

FIG. 4. The simulated Hall angle (a) as a function of δ_s driven by the right-handed and left-handed spin waves for $\omega_h = 300$ GHz, where the lines and symbols indicate the analytical and simulated results, and (b) as a function of ω_h driven by the right-handed spin waves for various δ_s.

and LLG simulated results, which exhibit a δ_s regime in which the theory coincides well with simulations. In detail, for the right- (left-) handed wave mode, the theory works well for $\delta_s > -0.2\,\mathrm{J\,s/m^3}$ ($\delta_s < 0.2\,\mathrm{J\,s/m^3}$). With the increase of positive δ_s, the FM term enhances significantly with the suppression of the AFM term. Moreover, the two terms contribute to the transverse motion along the $+y$ direction, while they compete with each other in relation to the longitudinal motion. As a result, the Hall angle increases gradually, and the skyrmion moves toward the spin wave source for $\delta_s > 0.3(\times 10^{-7}\,\mathrm{J\,s/m^3})$. When δ_s increases to ~1.24 where the FM term dominates, the skyrmion dynamics approaches that of the ferromagnetic skyrmion with topological number $Q = -1$ (depicted by the blue dashed arrow). However, there exists a δ_s regime in which the theory does not work [gray region in Fig. 4(a)]. In this δ_s regime, the energy of the wave mode is rather high, and the theory is not suitable to analyze the high-energy wave mode.

From the symmetry of the two-sublattice system, opposite Hall angles are expected for two FiM skyrmions with opposite δ_s driven by the left-handed and right-handed spin waves, respectively, which has been confirmed in our simulations. In Fig. 3(b), we present the skyrmion trajectory for various δ_s driven by the left-handed spin waves excited by magnetic field with $h = 1200$ mT. It is clearly shown that the trajectories of two skyrmions with opposite δ_s driven by the right-handed and left-handed spin waves, respectively [$\delta_s = 0.62$, for example, blue empty triangles in Fig. 3(a) and solid triangles in Fig. 3(b)], are symmetric around the x axis, demonstrating the opposite Hall angles for the two cases as shown in Fig. 4(a). It is clearly shown that the dependence of the Hall angle on $|\delta_s|$ driven by the left-handed spin waves is similar to the right-handed spin-wave-driven one.

So far, we have demonstrated theoretically and numerically that skyrmion Hall motion in a ferrimagnet highly depends on δ_s via tuning the ratio between two momentum terms acting on the skyrmion, allowing one to select suitable materials to better control the skyrmion motion. Furthermore, it is worth noting that the amplitude of the spin wave is also related to δ_s, while it hardly affects the skyrmion Hall angle.

Next, we check the effect of spin wave frequency ω_h on the skyrmion Hall motion. As a matter of fact, earlier work has reported that in ferromagnets and antiferromagnets, the increase of spin wave frequency at low wave number enhances the wave group velocity [15]. Thus, the effective Lorentz force is also increased, resulting in an enhanced skyrmion Hall motion. This property is also available in ferrimagnets. In Fig. 4(b), we present the simulated Hall angle as a function of ω_h for various δ_s at the wave number $\sim 0.2\,\mathrm{nm^{-1}}$, which clearly demonstrates the slight increase of the angle with the increasing ω_h regardless of the δ_s value.

E. Skyrmion driven by mixed-chirality spin waves

Finally, we investigate the interaction between a skyrmion and mixed-chirality spin waves which is likely more accessible in experiments. Here, the spin waves are composed of left-handed waves with a density ρ_L and right-handed waves with a density ρ_R.

In Fig. 5, we present the Bragg intensity from Fourier transformation of simulated n_x for three cases (I, $\rho_\mathrm{L} > \rho_\mathrm{R}$; II, $\rho_\mathrm{L} = \rho_\mathrm{R}$; and III, $\rho_\mathrm{L} < \rho_\mathrm{R}$ at $\delta_s = 0$). The left- and right-handed wave bands are scattered toward the positive and negative y directions, and the densities of the scattered waves are mainly determined by ρ_L and ρ_R, respectively. For example, for $\rho_\mathrm{L} = \rho_\mathrm{R}$ with an equal superposition of the left- and right-handed bands, the densities of the scattered waves are almost the same, as shown in Fig. 5(b). As a result, skyrmion Hall motion does not occur. Moreover, the scattered wave channels are asymmetric for $\rho_\mathrm{L} \neq \rho_\mathrm{R}$ [Figs. 5(a) and 5(c)], which induces a net transverse force and results in the skyrmion Hall motion even at $\delta_s = 0$, as shown in Fig. 6 where the simulated Hall angle as a function of δ_s for three cases is given.

Interestingly, the net angular momentum δ_s does efficiently modulate the skyrmion dynamics. For case II as an example, skyrmion Hall motion is induced and enhanced with increas-

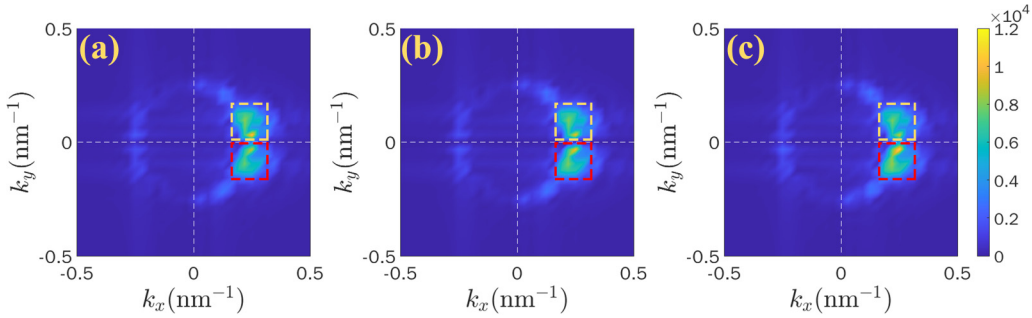

FIG. 5. Spatial fast Fourier transition spectrum for $\delta_s = 0$ driven by mixed-chirality spin waves for three cases, (a) $\rho_L > \rho_R$ ($h_R = 977$ mT, $h_L = 523$ mT), (b) $\rho_L = \rho_R$ ($h_R = 942$ mT, $h_L = 558$ mT), and (c) $\rho_L < \rho_R$ ($h_R = 900$ mT, $h_L = 600$ mT). The yellow (red) squares show the scattering of the left-handed (right-handed) spin waves.

ing $|\delta_s|$, as shown in Fig. 6 (red circles). On one hand, δ_s affects the FiM resonant frequency, which in turn tunes the spin wave density. Specifically, right-handed spin waves can be excited more easily than left-handed waves for a positive δ_s, while a negative δ_s tends to excite left-handed spin waves more easily, resulting in the mirror symmetry breaking of the scattered spin wave channels. On the other hand, δ_s also alters the skyrmion momentum and modulates the skyrmion dynamics, as discussed in Sec II D. Thus, both the spin wave excitation and momentum transfer are related to δ_s, resulting in the enhancement of the Hall motion as $|\delta_s|$ increases. Moreover, for cases I and III, the Hall motion could be suppressed for a particular δ_s (empty triangle and square in Fig. 6) at which the scattered wave channels are symmetric. To some extent, this effect could be used to eliminate skyrmion Hall motion through tuning δ_s.

F. Connection with experiments

It is noted that wave packet theory is no longer valid if the size of the wave packet at low frequency is larger than the skyrmion size [15]. Moreover, the linear spin wave theory which is based on the perturbation theory may not work well for spin waves with a large amplitude. Thus, in this work, we are mainly concerned with the waves with high frequency and low amplitude to obtain reasonable results and a conclusion.

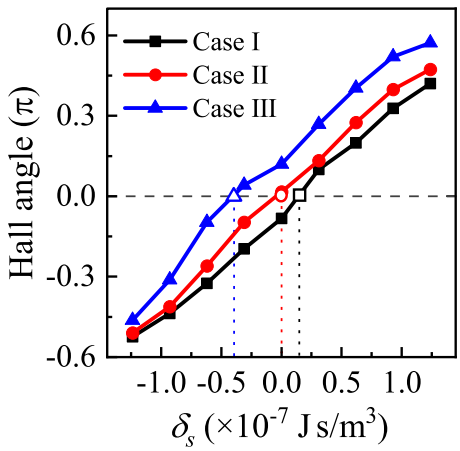

FIG. 6. The simulated Hall angle as a function of δ_s driven by the mixed-chirality spin waves for three cases.

Actually, one may estimate the speed of the skyrmion to provide more guidance for experiments, noting that the parameters considered in this work are comparable with those in GdFeCo. Specifically, a speed of ∼320 m/s is obtained for $\delta_s = 0.31$ (10^{-7} J s/m^3), comparable with that driven by an electric current [12]. Thus, the spin wave is revealed to be an efficient stimulus in driving skyrmions in ferrimagnets, which will be highly preferred in future low-power-consuming device design.

More importantly, δ_s has been proven to be a core control parameter in modulating the skyrmion Hall motion, allowing one to better control the skyrmion dynamics through tuning the δ_s value in ferrimagnets [52]. For example, suitable δ_s can be adjusted by ion doping to suppress the skyrmion Hall motion, which is of great importance for future applications considering the detrimental effect of Hall motion on data propagation. Of course, the prediction of spin-wave-driven skyrmion dynamics in a ferrimagnet given in the work deserves to be checked in further experiments.

IV. CONCLUSION

In conclusion, we have studied theoretically and numerically the skyrmion dynamics in ferrimagnets driven by circularly polarized spin waves. The spin wave scattering highly depends on its chirality, and the scattering direction is hardly affected by the net angle momentum δ_s. Interestingly, δ_s determines the ratio between the two spin wave induced momentum terms acting on the skyrmion, which in turn significantly affects the skyrmion Hall motion. The dependence of the Hall angle on δ_s and spin wave frequency is unveiled by numerical simulations, which demonstrate antiferromagnetic dynamics at $\delta_s = 0$ and ferromagneticlike dynamics for large δ_s. More importantly, the gradual transition in Hall angle on δ_s allows one to select suitable materials to better control the skyrmion motion, which is very meaningful for future spintronic applications.

ACKNOWLEDGMENTS

The work is supported by the Natural Science Foundation of China (Grants No. 51971096, No. 92163210, and No. 51721001), and the Guangdong Basic and Applied Basic Research Foundation (Grant No. 2022A1515011727).

[1] X. S. Wang, H. Y. Yuan, and X. R. Wang, A theory on skyrmion size, Commun. Phys. **1**, 31 (2018).

[2] L. Caretta, M. Mann, F. Büttner, K. Ueda, B. Pfau, C. M. Günther, P. Hessing, A. Churikova, C. Klose, M. Schneider, D. Engel, C. Marcus, D. Bono, K. Bagschik, S. Eisebitt, and G. S. D. Beach, Fast current-driven domain walls and small skyrmions in a compensated ferrimagnet, Nat. Nanotechnol. **13**, 1154 (2018).

[3] Y. Wang, L. Wang, J. Xia, Z. Lai, G. Tian, X. Zhang, Z. Hou, X. Gao, W. Mi, C. Feng, M. Zeng, G. Zhou, G. Yu, G. Wu, Y. Zhou, W. Wang, X.–x. Zhang, and J. Liu, Electric-field-driven non-volatile multi-state switching of individual skyrmions in a multiferroic heterostructure, Nat. Commun. **11**, 3577 (2020).

[4] Z. Hou, Y. Wang, X. Lan, S. Li, X. Wan, F. Meng, Y. Hu, Z. Fan, C. Feng, M. Qin, M. Zeng, X. Zhang, X. Liu, X. Fu, G. Yu, G. Zhou, Y. Zhou, W. Zhao, X. Gao, and J. Liu, Controlled switching of the number of skyrmions in a magnetic nanodot by electric fields, Adv. Mater. **34**, 2107908 (2022).

[5] L. J. Bannenberg, H. Wilhelm, R. Cubitt, A. Labh, M. P. Schmidt, E. Lelièvre-Berna, C. Pappas, M. Mostovoy, and A. O. Leonov, Multiple low-temperature skyrmionic states in a bulk chiral magnet, npj Quantum Mater. **4**, 11 (2019).

[6] X. Yao, Z. Wang, M. Deng, Z. X. Li, Z. Zhang, Y. Cao, and P. Yan, Magnetic skyrmion generation by reflective spin wave focusing, Front. Phys. **9**, 729967 (2021).

[7] S. Woo, K. M. Song, X. Zhang, M. Ezawa, Y. Zhou, X. Liu, M. Weigand, S. Finizio, J. Raabe, M. C. Park, K. Y. Lee, J. W. Choi, B. C. Min, H. C. Koo, and J. Chang, Deterministic creation and deletion of a single magnetic skyrmion observed by direct time-resolved x-ray microscopy, Nat. Electron. **1**, 288 (2018).

[8] X. Zhang, Y. Zhou, K. M. Song, T. E. Park, J. Xia, M. Ezawa, X. Liu, W. Zhao, G. Zhao, and S. Woo, Skyrmion-electronics: Writing, deleting, reading and processing magnetic skyrmions toward spintronic applications, J. Phys.: Condens. Matter **32**, 143001 (2020).

[9] G. Yin, Y. Li, L. Kong, R. K. Lake, C. L. Chien, and J. Zang, Topological charge analysis of ultrafast single skyrmion creation, Phys. Rev. B **93**, 174403 (2016).

[10] L. Peng, Y. Zhang, M. He, B. Ding, W. Wang, H. Tian, J. Li, S. Wang, J. Cai, G. Wu, J. P. Liu, M. J. Kramer, and B. Shen, Generation of high-density biskyrmions by electric current, npj Quantum Mater. **2**, 30 (2017).

[11] C. Jin, C. Song, J. Wang, and Q. Liu, Dynamics of antiferromagnetic skyrmion driven by the spin Hall effect, Appl. Phys. Lett. **109**, 182404 (2016).

[12] S. Woo, K. M. Song, X. Zhang, Y. Zhou, M. Ezawa, X. Liu, S. Finizio, J. Raabe, N. J. Lee, S. Il Kim, S. Y. Park, Y. Kim, J. Y. Kim, D. Lee, O. Lee, J. W. Choi, B. C. Min, H. C. Koo, and J. Chang, Current-driven dynamics and inhibition of the skyrmion Hall effect of ferrimagnetic skyrmions in GdFeCo films, Nat. Commun. **9**, 959 (2018).

[13] I. Lemesh and G. S. D. Beach, Walker Breakdown with a Twist: Dynamics of Multilayer Domain Walls and Skyrmions Driven by Spin-Orbit Torque, Phys. Rev. Appl. **12**, 044031 (2019).

[14] Z. Wang, H. Y. Yuan, Y. Cao, Z. X. Li, R. A. Duine, and P. Yan, Magnonic Frequency Comb through Nonlinear Magnon-Skyrmion Scattering, Phys. Rev. Lett. **127**, 037202 (2021).

[15] M. W. Daniels, W. Yu, R. Cheng, J. Xiao, and D. Xiao, Topological spin Hall effects and tunable skyrmion Hall effects in uniaxial antiferromagnetic insulators, Phys. Rev. B **99**, 224433 (2019).

[16] X. Liang, J. Xia, X. Zhang, M. Ezawa, O. A. Tretiakov, X. Liu, L. Qiu, G. Zhao, and Y. Zhou, Antiferromagnetic skyrmion-based logic gates controlled by electric currents and fields, Appl. Phys. Lett. **119**, 062403 (2021).

[17] X. Zhang, J. Xia, K. Shirai, H. Fujiwara, O. A. Tretiakov, M. Ezawa, Y. Zhou, and X. Liu, Configurable pixelated skyrmions on nanoscale magnetic grids, Commun. Phys. **4**, 255 (2021).

[18] J. Tang, Y. Wu, W. Wang, L. Kong, B. Lv, W. Wei, J. Zang, M. Tian, and H. Du, Magnetic skyrmion bundles and their current-driven dynamics, Nat. Nanotechnol. **16**, 1086 (2021).

[19] J. Iwasaki, M. Mochizuki, and N. Nagaosa, Universal current-velocity relation of skyrmion motion in chiral magnets, Nat. Commun. **4**, 1463 (2013).

[20] W. Wang, M. Beg, B. Zhang, W. Kuch, and H. Fangohr, Driving magnetic skyrmions with microwave fields, Phys. Rev. B **92**, 020403(R) (2015).

[21] S. Abdizadeh, J. Abouie, and K. Zakeri, Dynamical switching of confined magnetic skyrmions under circular magnetic fields, Phys. Rev. B **101**, 024409 (2020).

[22] J. J. Liang, J. H. Yu, J. Chen, M. H. Qin, M. Zeng, X. B. Lu, X. S. Gao, and J. M. Liu, Magnetic field gradient driven dynamics of isolated skyrmions and antiskyrmions in frustrated magnets, New J. Phys. **20**, 053037 (2018).

[23] L. Shen, J. Xia, G. Zhao, X. Zhang, M. Ezawa, O. A. Tretiakov, X. Liu, and Y. Zhou, Dynamics of the antiferromagnetic skyrmion induced by a magnetic anisotropy gradient, Phys. Rev. B **98**, 134448 (2018).

[24] R. Tomasello, S. Komineas, G. Siracusano, M. Carpentieri, and G. Finocchio, Chiral skyrmions in an anisotropy gradient, Phys. Rev. B **98**, 024421 (2018).

[25] H. Yu, J. Xiao, and H. Schultheiss, Magnetic texture based magnonics, Phys. Rep. **905**, 1 (2021).

[26] P. Yan, X. S. Wang, and X. R. Wang, All-Magnonic Spin-Transfer Torque and Domain Wall Propagation, Phys. Rev. Lett. **107**, 177207 (2011).

[27] J. Xiao and G. E. W. Bauer, Spin-Wave Excitation in Magnetic Insulators by Spin-Transfer Torque, Phys. Rev. Lett. **108**, 217204 (2012).

[28] J. H. Moon, S. M. Seo, K. J. Lee, K. W. Kim, J. Ryu, H. W. Lee, R. D. McMichael, and M. D. Stiles, Spin-wave propagation in the presence of interfacial Dzyaloshinskii-Moriya interaction, Phys. Rev. B **88**, 184404 (2013).

[29] S. H. Oh, S. K. Kim, J. Xiao, and K. J. Lee, Bidirectional spin-wave-driven domain wall motion in ferrimagnets, Phys. Rev. B **100**, 174403 (2019).

[30] E. G. Tveten, A. Qaiumzadeh, and A. Brataas, Antiferromagnetic Domain Wall Motion Induced by Spin Waves, Phys. Rev. Lett. **112**, 147204 (2014).

[31] R. Cheng, M. W. Daniels, J.-G. Zhu, and D. Xiao, Antiferromagnetic spin wave field-effect transistor, Sci. Rep. **6**, 24223 (2016).

[32] J. Lan and J. Xiao, Skew scattering and side jump of spin wave across magnetic texture, Phys. Rev. B **103**, 054428 (2021).

[33] J. Iwasaki, A. J. Beekman, and N. Nagaosa, Theory of magnon-skyrmion scattering in chiral magnets, Phys. Rev. B **89**, 064412 (2014).

[34] H. Y. Yuan, Z. Yuan, R. A. Duine, and X. R. Wang, Recent progress in antiferromagnetic dynamics, EPL **132**, 57001 (2020).

[35] Z. Jin, C. Y. Meng, T. T. Liu, D. Y. Chen, Z. Fan, M. Zeng, X. B. Lu, X. S. Gao, M. H. Qin, and J. M. Liu, Magnon-driven skyrmion dynamics in antiferromagnets: Effect of magnon polarization, Phys. Rev. B **104**, 054419 (2021).

[36] V. V. Yurlov, K. A. Zvezdin, P. N. Skirdkov, and A. K. Zvezdin, Domain wall dynamics of ferrimagnets influenced by spin current near the angular momentum compensation temperature, Phys. Rev. B **103**, 134442 (2021).

[37] S. K. Kim, K. J. Lee, and Y. Tserkovnyak, Self-focusing skyrmion racetracks in ferrimagnets, Phys. Rev. B **95**, 140404(R) (2017).

[38] K. J. Kim, S. K. S. Kim, Y. Hirata, S. H. Oh, T. Tono, D. H. Kim, T. Okuno, W. S. Ham, S. K. S. Kim, G. Go, Y. Tserkovnyak, A. Tsukamoto, T. Moriyama, K. J. Lee, and T. Ono, Fast domain wall motion in the vicinity of the angular momentum compensation temperature of ferrimagnets, Nat. Mater. **16**, 1187 (2017).

[39] S. H. Oh, S. K. Kim, D. K. Lee, G. Go, K. J. Kim, T. Ono, Y. Tserkovnyak, and K. J. Lee, Coherent terahertz spin-wave emission associated with ferrimagnetic domain wall dynamics, Phys. Rev. B **96**, 100407(R) (2017).

[40] S. K. Kim, K. Nakata, D. Loss, and Y. Tserkovnyak, Tunable Magnonic Thermal Hall Effect in Skyrmion Crystal Phases of Ferrimagnets, Phys. Rev. Lett. **122**, 057204 (2019).

[41] S. K. Kim, G. S. D. Beach, K.-J. Lee, T. Ono, T. Rasing, and H. Yang, Ferrimagnetic spintronics, Nat. Mater. **21**, 24 (2022).

[42] Y. Onose, Y. Okamura, S. Seki, S. Ishiwata, and Y. Tokura, Observation of Magnetic Excitations of Skyrmion Crystal in a Helimagnetic Insulator Cu_2OSeO_3, Phys. Rev. Lett. **109**, 037603 (2012).

[43] S. Ding, A. Ross, R. Lebrun, S. Becker, K. Lee, I. Boventer, S. Das, Y. Kurokawa, S. Gupta, J. Yang, G. Jakob, and M. Kläui, Interfacial Dzyaloshinskii-Moriya interaction and chiral magnetic textures in a ferrimagnetic insulator, Phys. Rev. B **100**, 100406(R) (2019).

[44] H. Wu, F. Groß, B. Dai, D. Lujan, S. A. Razavi, P. Zhang, Y. Liu, K. Sobotkiewich, J. Förster, M. Weigand, G. Schütz, X. Li, J. Gräfe, and K. L. Wang, Ferrimagnetic skyrmions in topological insulator/ferrimagnet heterostructures, Adv. Mater. **32**, 2003380 (2020).

[45] W. H. Li, Z. Jin, D. L. Wen, X. M. Zhang, M. H. Qin, and J. M. Liu, Ultrafast domain wall motion in ferrimagnets induced by magnetic anisotropy gradient, Phys. Rev. B **101**, 024414 (2020).

[46] M. W. Daniels, R. Cheng, W. Yu, J. Xiao, and D. Xiao, Nonabelian magnonics in antiferromagnets, Phys. Rev. B **98**, 134450 (2018).

[47] Z. Y. Chen, M. H. Qin, and J. M. Liu, Ultrafast depinning of domain walls in notched antiferromagnetic nanostructures, Phys. Rev. B **100**, 020402(R) (2019).

[48] E. G. Tveten, T. Müller, J. Linder, and A. Brataas, Intrinsic magnetization of antiferromagnetic textures, Phys. Rev. B **93**, 104408 (2016).

[49] D. H. Kim, S. H. Oh, D. K. Lee, S. K. Kim, and K. J. Lee, Current-induced spin-wave Doppler shift and attenuation in compensated ferrimagnets, Phys. Rev. B **103**, 014433 (2021).

[50] G. G. Scott, Review of gyromagnetic ratio experiments, Rev. Mod. Phys. **34**, 102 (1962).

[51] T. Nan, H. Lin, Y. Gao, A. Matyushov, G. Yu, H. Chen, N. Sun, S. Wei, Z. Wang, M. Li, X. Wang, A. Belkessam, R. Guo, B. Chen, J. Zhou, Z. Qian, Y. Hui, M. Rinaldi, M. E. McConney, B. M. Howe *et al.*, Acoustically actuated ultra-compact NEMS magnetoelectric antennas, Nat. Commun. **8**, 296 (2017).

[52] Y. Hirata, D. H. Kim, S. K. Kim, D. K. Lee, S. H. Oh, D. Y. Kim, T. Nishimura, T. Okuno, Y. Futakawa, H. Yoshikawa, A. Tsukamoto, Y. Tserkovnyak, Y. Shiota, T. Moriyama, S. B. Choe, K. J. Lee, and T. Ono, Vanishing skyrmion Hall effect at the angular momentum compensation temperature of a ferrimagnet, Nat. Nanotechnol. **14**, 232 (2019).